25th ABCM International Congress of Mechanical Engineering
October 20-25, 2019, Uberlândia, MG, Brazil

CCOB-2019-1081
RADIAL INFLOW MICROTURBINE MODELING FOR ORGANIC RANKINE CYCLE

Richardson Leandro Nunes
Guilherme Scagnolatto
Gustavo Moraes Coraça
Cristiano Bigonha Tibiriçá
Luben Cabezas Gómez
Universidade de São Paulo – Câmpus de São Carlos. Av. Trabalhador São-carlense, 400, Arnold Schimidt.São Carlos – São Paulo – Brazil – CEP 13.566-590
eng.richard.nunes@gmail.com
guilherme.scagnolatto@usp.br
gustavo.coraca@usp.br
bigonha@sc.usp.br
lubencg@sc.usp.br

Abstract. *Traditionally, Rankine cycles use water as working fluid and high temperature energy sources, above 370°C, mainly steam boilers. In Organic Rankine Cycle organic fluids are used with lower evaporation temperatures and pressures than water, allowing the use of heat from several sources with lower temperatures (between 60 and 250°C) for electricity generation. The main objective was use a model of radial inflow turbine coupled with a Organic Rankine cycle (ORC) model to analyze the influence of various parameters (flow coefficient, mass flow, angular speed and turbine inlet pressure) on the size of turbine and cycle net electric power output. The speed of turbine ω and mass flow rate $\dot{m}$ are the main parameters of influence in performance. Choice of working fluid can also significantly influence turbine and cycle performance*

Keywords: *ORC, radial inflow turbine, micro-scale, R245fa, R123*

1. INTRODUCTION

Traditionally, Rankine cycles use water as working fluid that needs high temperature energy sources, above 370°C, mainly steam boilers. In Organic Rankine Cycle organic fluids are used with lower evaporation temperatures and pressures than water, allowing to generate electricity from several sources with lower temperatures (between 60 and 250°C), such as waste heat recovery, geothermal, solar and others. The Rankine cycle operates between a hot source of heat and a cold sink, producing mechanical work. For this process to occur, we have some basic components: the pump, the heater or evaporator, the expander and the condenser. These components have influence on Rankine cycle performance. Once the heat source is set for the cycle, the maximum evaporation temperature will also be set by the knowledge of source temperature. After that it can be selected a working fluid that is best suited to the temperature range. The selected fluid will influence factors such as evaporation pressure, condensation pressure, equipment size due to its specific volume, etc.

Equipments of the cycle also have a direct influence on performance. Among the various equipment of the cycle, the turbine is the one that most influences performance of the cycle, due to the large irreversibility inherent to its operation and also due to the variation of performance in various working ranges. Axial turbines are best suited for high mass flow rates and low pressure ratios, radial turbines achieve higher pressure ratios for lower flow rates and are therefore better suited for ORC systems (BAO, ZHAO, 2013). This work focuses to use a methodology of calculation of radial inflow micro turbines elaborated by Rahbar et al (2014) to obtain the basic constructive features of a turbine and to test the influence of several parameters, such as flow coefficient ϕ, mass flow $\dot{m}$, turbine inlet pressure $P_{t,1}$, angular velocity ω. In section 2 the turbine modeling approach is presented. In section 3 are presented the results obtained simulating the variation of the parameters. Finally, in section 4 the discussions and conclusions are presented.

2. MODELING PROCEDURE

In Fig. 1a) it can be seen the schematic flow chart of the system operating with Organic Rankine Cycle (ORC). The organic fluid in the vapor condition at point 1 enters the turbine where it will be expanded to point 5, where it enters the

condenser and exits condensed at point 6, where it is pumped into the evaporator where it will be heated and evaporated, returning at point 1 where the cycle repeats. The processes inside turbine are shown in Fig. 1b. It can be seen the points of the cycle and greater attention is given to the points at the entrance, exit and inside the turbine. Points 1, 5, 6 and 7 are the same as those given in Fig. 1 a). Point 1 is still the turbine inlet, point 2 is the outlet of the volute and nozzle inlet, point 3 is the outlet of the nozzle, point 4 is the inlet of the rotor and point 5 is the outlet of the rotor. Between point 3 and point 4 is the gap space between rotor and nozzle.

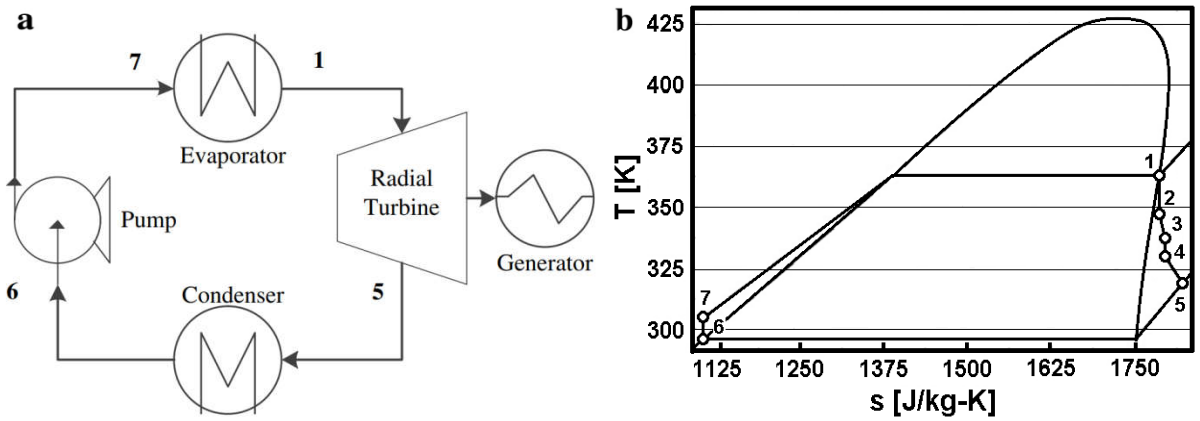

Figure 1 a) Flow chart of the ORC cycle b) Diagram of the processes.

The turbine is composed of three parts: volute, rotor and nozzle. Process of the cycle can be seen in the T-s diagram of Fig. 2. In process 1-2, the fluid enters volute and is evenly distributed. In process 2-3, the fluid is accelerated, gaining circumferential speed in the nozzle. In process 3-4, the fluid across interspaced between nozzle and rotor. In process 4-5, the kinetic and thermal energy is converted by rotor's movement, slowdown and expansion of fluid. The mean line model is used for calculate the turbine. This is a one-dimensional method where fluid physical and thermodynamic properties are assumed constant in a cross section normal to direction of fluid flow and in specific interest points. To obtain the properties, it is used the Euler equation of turbo machines, the principles of mass, energy and momentum conservation. Losses in fluid flow and blocking factor are also considered.

The input data are the total temperature $T_{t,1}$, the total pressure $P_{t,1}$, the static total pressure ratio ER_{ts}, turbine speed ω, geometry ratios and non-dimensional parameters such as load coefficient ψ, flow coefficient ϕ, swirl coefficient SC, the volute loss coefficient k_{voluta}, blocking factor BK, temperature of the heat source $T_{heatsouce}$, Δt_{eva}, pump electrical-mechanical efficiency η_{pump}, generator efficiency $\eta_{generator}$, turbine mechanical efficiency η_{mec} and mass flow of fluid $\dot{m}$. The input parameters are summarized in table 1.

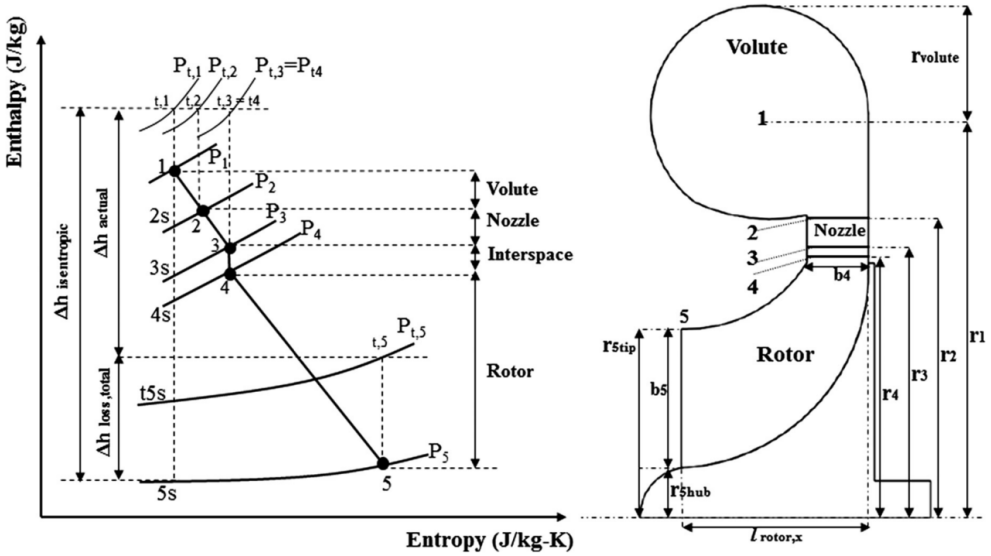

Figure 2 Diagram h-s of the process in turbine and cross section of the turbine.

The model considers four elements: rotor; nozzle and rotor-nozzle interspace; volute; and initial efficiency estimation and performance parameters. The modeling approach follows the reverse path of fluid flow, where fluid enters the volute, crosses the nozzle, enters the rotor-nozzle interspace, crosses the rotor, and leaves the turbine.

Table 1 Input parameters of the model.

Parameter	Units	Range	Reference
Volute inlet total temperature $T_{t,1}$	K	423	Clemente *et al* (2013) Sauret *et al* (2011) Fiaschi *et al* (2012)
Volute inlet total pressure $P_{t,1}$	kPa	200 to 3460	Clemente *et al* (2013) Sauret *et al* (2011) Fiaschi *et al* (2012)
Total-static pressure ratio ER_{ts}	-	2 to 15	Clemente *et al* (2013) Sauret *et al* (2011) Fiaschi *et al* (2012)
Turbine speed ω	Rpm	30000 to 70000	Sauret *et al* (2011) Fiaschi *et al* (2012)
Loading coefficient ψ	-	0.8 to 2.4	Fiaschi *et al* (2012) Moustapha *et al* (2003)
Flow coefficient ϕ	-	0.2 to 0.5	Moustapha *et al* (2003)
Rotor exit absolute flow angle α_5	degrees	-15 to 15	Moustapha *et al* (2003)
Rotor exit hub to inlet radii ratio r_{5eixo}/r_4	-	0.2 to 0.3	Whitfield *et al* (1990) Moustapha *et al* (2003) Aungier (2006)
Nozzle inlet to exit radii ratio r_2/r_3	-	1.2 to 1.3	Moustapha *et al* (2003) Glassman *et al* (1976)
Volute swirl coefficient SC	-	0.95	Moustapha *et al* (2003)
Volute pressure loss coefficient k_{voluta}	-	0.1	Moustapha *et al* (2003)
Flow blockage factor BK	-	0.1	Moustapha *et al* (2003)
temperature of the heat source $T_{heatsouce}$	K	433	Sauret *et* al (2011) Fiaschi *et* al (2012)
Evaporator temperature difference Δt_{eva}	K	10	Sauret *et* al (2011)
pump electrical-mechanical efficiency η_{pump}	-	0.75	Hettiarachchi *et al* (2007)
generator efficiency $\eta_{generator}$	-	0.96	Hettiarachchi *et al* (2007)
turbine mechanical efficiency η_{mec}	-	0.96	Hettiarachchi *et al* (2007)
mass flow of fluid $\dot{m}$	Kg/s	0.2 to 1.8	Clemente *et* al (2013) Fiaschi *et* al (2012)

2.1 Turbine's rotor modeling

This model was implemented following Moustapha et al (2003), where two dimensionless parameters are needed, the load coefficient ψ and the flow coefficient ϕ. The first represents enthalpy drop of the turbine, the second represents the volumetric flow rate through turbine. Load coefficient is obtained from Eq. 1.

$$\psi = \Delta h_{actual} \,/\, U_4^2 = \Delta h_{actual} \,/\, (r_4.\omega)^2 \tag{1}$$

Flow coefficient is obtained from Eq.

$$\phi = C_{m5}/U_4 \tag{2}$$

Moustapha (2003) obtained several results from simulations using ψ and ϕ. The turbines simulated have mainly inlet temperatures of 600ºC to 1000ºC, i.e., have severe operating conditions due high speed and temperature. This problem is minimized using $\psi < 1$ and also for ψ. The use of the rotor blade inlet null angle also reduces this problem as the blade inlets are aligned radially. Fig. 3 shows a radial inlet centrifugal turbine with zero rotor blade inlet angles and also the speed triangle.

ORC turbines, on the other hand, operate at lower temperatures usually around 200 °C. This makes it easier for the blade inlet angle to be nonzero and to better adjust to the flow conditions at the rotor inlet, leading to better turbine performance. Fig. 3(a) shows a radial inlet centrifugal turbine with non-zero blade inlet angle and load coefficient values $\psi > 1$.

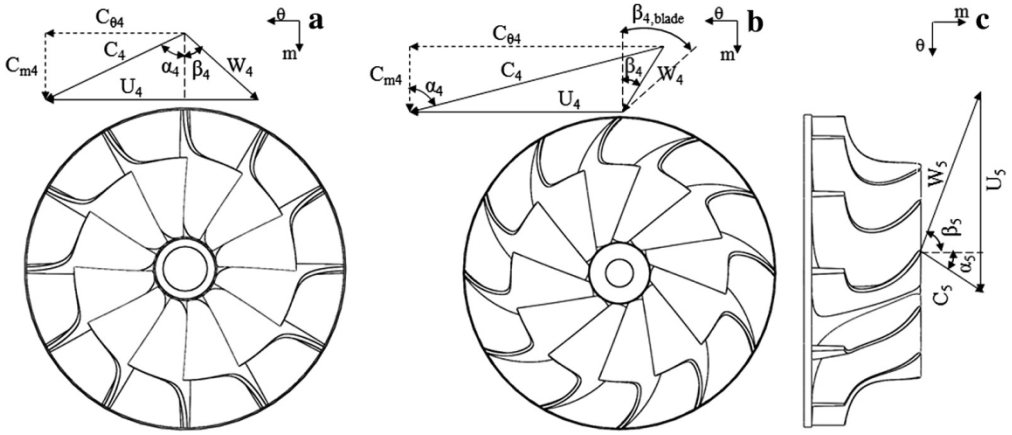

Figure 3 – Blade geometry and speed triangle of a radial inlet turbine with zero inlet blade angle. Source: Rahbar et al (2014).

The rotor of Fig. 3(b) has a more suitable angle at the blade inlets, aligning with the direction of fluid flow. This allows for the same tangential velocity U_4 to have greater tangential velocity $C_{\theta 4}$ than the rotor of Fig. 3(a). Considering the same output speeds (U_5 and C_5) for both and analyzing Eq. 3, it can be concluded that the rotor of Fig. 3(b) produces more actual specific work.

$$\Delta h_{actual} = U_4 C_{\theta 4} - U_5 C_{\theta 5} \tag{3}$$

With the total temperature $T_{t,1}$ and the total pressure $P_{t,1}$ as input data, the thermodynamic properties in state 1 are determined by Eq. 4.

$$(s_{t,1}, h_{t,1}) = Coolprop(T_{t,1}, P_{t,1}, fluid) \tag{4}$$

The outlet pressure P_5 may be calculated from Eq. 5.

$$P_5 = P_{5s} = P_{t,1} \,/\, ER_{ts} \tag{5}$$

Where P_{5s} is the pressure obtained by isoentropic expansion. The isentropic expansion point 5_s is then determined. At this point the entropy is the same as the entropy of state 1, as given in Eq. 6.

$$s_{5s} = s_{t,1} \tag{6}$$

Thus, the enthalpy h_{5s} is determined from Eq. 7.

$$(T_{5s}, h_{5s}) = Coolprop(s_{5s}, P_{5s}, fluid) \tag{7}$$

The enthalpy drop $\Delta h_{isentropic}$ is calculated by Eq. 8.

$$\Delta h_{isentropic} = h_{t,1} - h_{5s} \tag{8}$$

Using the estimated turbine efficiency for the first time, the actual enthalpy drop Δh_{actual} is calculated by Eq. 9.

$$\Delta h_{actual} = \Delta h_{isentropic} \cdot \eta_{turbine} \tag{9}$$

Turbine output power can be calculated from Eq. 10.

$$\dot{W}_{turbine} = \dot{m}_{fluid} \cdot \Delta h_{actual} \tag{10}$$

Assuming that an adiabatic process occurs from point 1 to point 4, we can consider the enthalpy remains the same as point 1 to 4, as in Eq. 11.

$$h_4 = h_{t,1} \tag{11}$$

The total and static thermodynamic properties at the rotor input ($t_{t,4}, s_{t,4}, h_{t,4}, \rho_{t,4}, T_4, h_4, \rho_4$) can be determined by Eq. 11, Coolprop, C_4, W_4 and Eq. 12, presented by Aungier et al (2006).

$$P_{t,4} = P_{t,1} - \rho_{t,1}.\Delta h_{actual}.(1 - \eta_{turbine}) \,/\, (4.\eta_{turbine}) \tag{12}$$

The thermodynamic properties on the rotor output ($P_{t,5}, T_{t,5}, s_{t,5}, \rho_{t,5}, T_5, \rho_5$) can be determined by considering the isentropic expansion point 5_s, Coolprop, C_5, W_5, and Eq. 13.

$$h_5 = \left(h_{t,4} - \Delta h_{actual}\right) - C_5^2 \,/\, 2 \tag{13}$$

Properties of the state 5 can be used in the ORC model to complete the cycle.
The rotor output area is given by Eq. 14.

$$A_5 = \dot{m} \,/\, (\rho_5.\phi.U_4.(1 - BK)) \tag{14}$$

BK is the blocking factor that accounts for the growth of boundary layers between rotor blade spaces.
The radius at the exit tip of rotor r_{5p} is obtained using the radius ratio r_{5axis}/r_4 provided as input data and using Eq. 15.

$$r_{5p} = \sqrt{A_5 \,/\, \pi + r_{5p}^2} \tag{15}$$

Using the correlation obtained by Glassman (1976) and expressed in Eq. 16, the number of Z_{rotor} rotor blades is calculated.

$$Z_{rotor} = (\pi \,/\, 30).(110 - \alpha_4).tg(\alpha_4) \tag{16}$$

The considered rotor losses are: tip clearance, secondary, friction and output kinetics. The loss of tip clearance is given by the equations Eq. 17, Eq. 18, Eq. 19 and Eq. 20, reported by Moustapha et al (2003).

$$C_x = \left(1 - r_{rp} \,/\, r_4\right) \,/\, (c_{m4}.b_4) \tag{17}$$
$$C_r = (r_{5p} \,/\, r_4).\left(l_{rotor,x} - b_4\right) \,/\, (c_{m5}.r_5.b_5) \tag{18}$$
$$l_{rotor,x} = 1{,}5.(r_{5p} - r_{5hub}) \tag{19}$$
$$\Delta h_{clearance} = U_4^3.Z_{rotor} \,/\, 8.\pi.(0{,}4.\epsilon_x.C_x + 0{,}75.\epsilon_r.C_r - 0{,}3.\sqrt{\epsilon_x.\epsilon_r, C_x.C_r}) \tag{20}$$

The coefficients ϵ_x and ϵ_r are given by Eq. 21 and Eq. 22.

$$\epsilon_x = 0{,}04.(r_{5p} - r_{5hub}) \tag{21}$$
$$\epsilon_r = \epsilon_x \tag{22}$$

Secondary losses and friction losses are obtained from Eq. 23 and Eq. 24, as in Suhrmann et al (2010).

$$\Delta h_{secundary} = (C_4^2.d_4) \,/\, (Z_{rotor}.r_c) \tag{23}$$

$$\Delta h_{fricton} = f.\left(1 + 0{,}075.\overline{Re}^{0{,}25}.\sqrt{\frac{d_{hydraulic}}{2.r_c}}\right).\left[Re.\left(\frac{d_4}{2.r_c}\right)^2\right]^{0{,}05}.\left[\frac{W_4 + \left(\frac{W_{5p} + W_{5hub}}{2}\right)}{2}\right]^2.\frac{l_{hydraulic}}{d_{hydraulic}} \tag{24}$$

The friction factor used in Eq. 24 is given by Churchill's (1977) Eq. 25.

$$f = 8.\left(\left(\frac{8}{\overline{Re}}\right)^{12} + \left(\left[2{,}457.\ln\left(\frac{1}{\left(\frac{7}{\overline{Re}}\right)^{0{,}9} + 0{,}27.RR}\right)\right]^{16} + \left(\frac{37530}{\overline{Re}}\right)_{16}\right)^{-1{,}5}\right)^{\frac{1}{12}} \tag{25}$$

RR is the relative surface roughness, considering $RR = 0.0002m$ as used by Aungier (2006).
$\overline{Re}$ is used as the average number of Reynolds from inlet to turbine outlet, calculated by Eq. 26.

$$\overline{Re} = \left[U_4.b_4.\rho_4 \,/\, \mu_4 + U_5.\left(r_{5p} - r_{5hub}\right).\rho_5 \,/\, \mu_5\right]/2 \tag{26}$$

The hydraulic length $l_{hydraulic}$ is given by Eq. 27, according to Rahbar (2014).

$$l_{hydraulic} = (\pi\,/2\,).\left(\sqrt{\left(r_4 - r_{5p} + b_4\,/2\right)^2 + \left((r_{5p} - r_{5hub})\,/2\right)^2}\right)/2 \tag{27}$$

The hydraulic diameter $d_{hydraulic}$ is calculated by Eq. 28, as realized by Rahbar (2014).

$$d_{hydraulic} = 0{,}5.\left(\frac{4.\pi.r_4.b_4}{2.\pi.r_4 + Z_{rotor}.b_4} + \frac{2.\pi.\left(r_{5p}^2 - r_{5hub}^2\right)}{\pi.\left(r_{5p} - r_{5hub}\right) + Z_{rotor}.\left(r_{5p} - r_{5hub}\right)}\right) \tag{28}$$

Suhmann et al (2010) provides Eq. 29 for the energy loss due to wasted kinetic energy at the rotor output.

$$\Delta h_{exit} = 0{,}5.C_5^2 \tag{29}$$

2.2 Turbine's nozzle and interspace between rotor and nozzle modeling

The losses that occur in interspace are small relative to the losses that occur in rotor and nozzle, so that an isentropic process can be assumed to occur in interspace, that is given by Eq. 30.

$$s_3 = s_4 \tag{30}$$

From Eq. 30, conservation of mass, conservation of angular momentum, thermodynamic properties at rotor inlet and Eq. 31, iteratively calculated at the nozzle outlet (point 3): thermodynamic properties, absolute velocity C_3 and the geometry.

$$r_3 = r_4 + 2.b_4.\cos\left(\alpha_4\right) \tag{31}$$

Using the nozzle inlet and outlet radius ratio $r_2\,/\,r_3$ and the conditions calculated at the nozzle outlet, the geometry and thermodynamic properties at the nozzle outlet are calculated.
Nozzle friction loss is presented by Whitfield et al (1990) in Eq. 32.

$$\Delta h_{friction,nozzle} = 4.f_{nozzle}.\bar{C}^2.\frac{r_2 - r_3}{d_{hydraulic,nozzle}} \tag{32}$$

The hydraulic diameter $d_{hydraulic,nozzle}$ of Eq. 3.32 is obtained from Eq. 3.33.

$$d_{hydraulic,nozze} = \frac{1}{2}.\left(\frac{8.\pi.r_2.b_4.\cos(\alpha_2)}{4.\pi.r_2 + \frac{4.\pi.b_4.r_2}{\sigma}} + \frac{8.\pi.r_3.b_4.\cos(\alpha_3)}{4.\pi.r_3 + \frac{(4.\pi.b_4.r_3)}{\sigma}}\right) \tag{33}$$

The average Reynolds number on the $\overline{Re}_{nozzle}$ nozzle is calculated by Eq. 3.34.

$$\overline{Re}_{nozzle} = \left(\frac{U_2.b_4.\rho_2}{\mu_2} + \frac{U_3.b_4.\rho_3}{\mu_3}\right)/2 \tag{34}$$

2.3 Turbine's volute modeling

The width b_4 is assumed constant along the length of the nozzle. Glassman (1976) presents $\sigma = 1.35$.

$$A_1 = \dot{m}_{fluid}\,/\,(\rho_1.C_1) \tag{35}$$
$$r_1 = (r_2.C_{\theta 2})\,/(SC.C_1) \tag{36}$$
$$r_{volute} = \sqrt{A_1\,/(0{,}75.\pi + 1)} \tag{37}$$

The swirl coefficient SC represents the friction effect on the volute surface and is given by Eq. 38.

$$d_{max} = 2.(r_1 + r_{volute}) \tag{38}$$

Volute losses are obtained in Eq. 39.

$$\Delta h_{loss,volute} = k_{volute}.C_2^2\ /2 \tag{39}$$

The pressure loss coefficient is considered $k_{volute} = 0.1$ as used by Moustapha et al (2003).

2.4 Turbine's efficiency estimation and performance parameters

Total turbine losses are obtained by summing all losses in Eq. 40.

$$\Delta h_{loss,total} = \Delta h_{loss,volute} + \Delta h_{friction,nozze} + \Delta h_{tip,clearance} + \Delta h_{secundary} + \Delta h_{friction} + \Delta h_{exit} \tag{40}$$

Thus the efficiency of the turbine can be calculated from Eq. 41.

$$\eta_{turbine,ts} = \Delta h_{actual}\ /(\Delta h_{actual} + \Delta h_{loss,total}) \tag{41}$$

This obtained efficiency value is used at the beginning of the turbine model calculations at the beginning of this chapter, iterating until the value converges to the specified tolerance η_{tol}. Eq. 42 provides the turbine reaction.

$$R = (h_4 - h_5)/\ (h_{t,1} - h_{t,5}) \tag{42}$$

The specific angular velocity N_s is given by Eq. 43

$$N_s = (\omega.\sqrt{C_{m5}.A_5})/(\Delta h_s)^{0,75} \tag{43}$$

The velocity ratio v is obtained from Eq. 44

$$v = U_4\ /\ \sqrt{2.\Delta h_s} \tag{44}$$

2.5 Integrating ORC modeling and turbine modeling

The ORC cycle is calculated by determining the points of the Fig. 1 a) as in flow chart of the Fig. 4. Start from point 6, where P_6 is the condensation pressure and fluid is in saturated liquid state, so the properties are determined. P_7 is the evaporation pressure. Between point 6 and 7 occur an isentropic pressurization, so state 7 is determined from P_7 and h_7 and the properties are obtained. P_1 is the evaporation pressure, T_1 is an input, so the state 1 is determined. P_5 is the evaporation pressure, s_5 is obtained gathering an isentropic expansion and the η_{turb}, thus the state 5 is determined.

The model starts with the input data of the cycle and the turbine of the Table 1 (fluid conditions and geometric parameters of the turbine) e following the flow chart of the Fig. 5: An initial efficiency is estimated to start the process. Then the turbine is calculated (fluid conditions, losses, geometries) in parts: rotor, gap space, nozzle and volute. A new efficiency is obtained and compared to the previous value. This process is repeated iteratively by the method of successive approximations until the efficiency reaches the desired convergence. With the turbine calculated geometrically and thermodynamically and point 5 is known, the state 6 is calculated by means of cooling and isobaric condensation. Then point 7 is calculated with a pumping (pressure increase). State 1 is known, then the power supplied to the system by the heat source is calculated. Through the work produced in the generator from the work done by the turbine, the work consumed by the pump and the energy supplied to the system, the net work of the system is obtained.

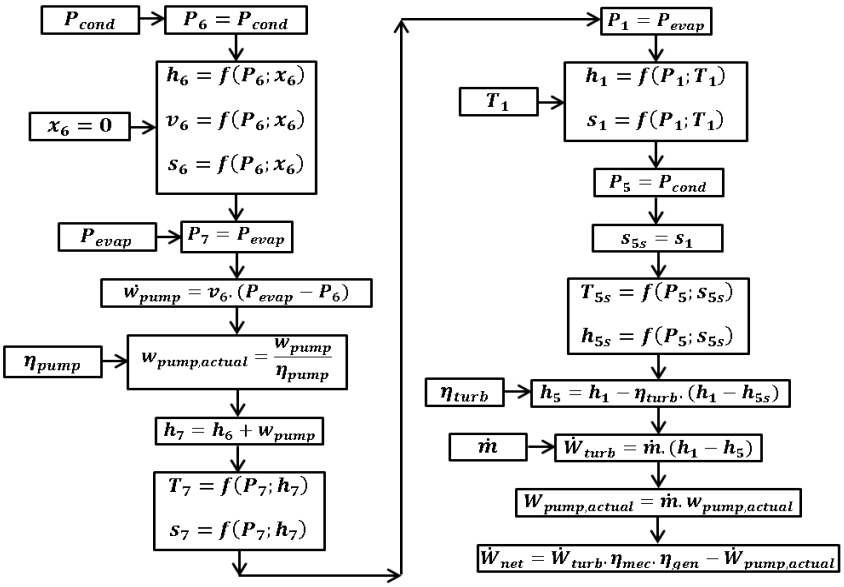

Figure 4. Flow chart of ORC modeling

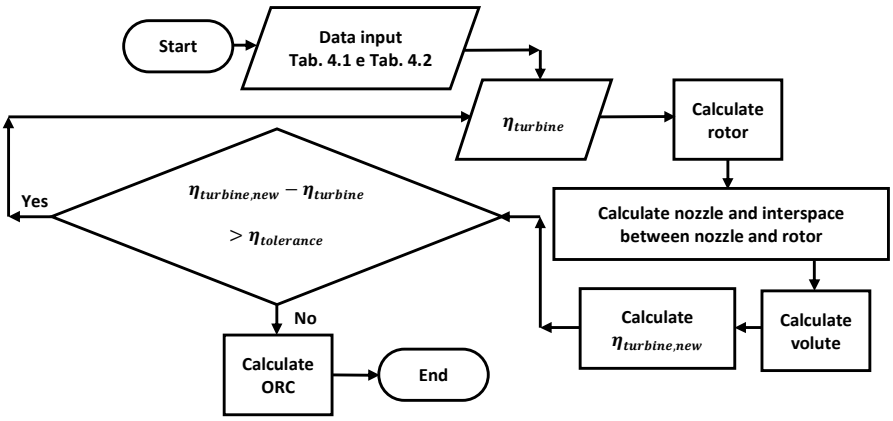

Figure 5. Flow chart of the turbine and ORC integrated

3. RESULTS

Simulations were carried out to verify the influence of several parameters on the size of the turbine and on the liquid work produced in the system. The simulations were based on the simulations of Rahbar et al (2014). Fig. 6 shows the influence of the flow coefficient on the size of the turbine and on the liquid work produced in the cycle. As illustrated in Fig. 6, only the cycle net electric power output $\dot{W}_{net}$ is affected by the variation of flow coefficient ϕ. Increasing ϕ leads to larger absolute meridional velocity at rotor exit C_{m5} based on Eq. 2. The larger the C_{m5} the larger is the exit kinetic loss (Eq. 29) and consequently lower turbine efficiencies $\eta_{turbine}$ are obtained based on Eq. 40 and Eq. 41. Since $\Delta h_{isoentropic}$ is fixed by the $T_{t,1}$ and ER_{ts}, reduction in $\eta_{turbine}$ results in smaller actual enthalpy drop and consequently smaller W_{net} is achieved

Figure 7 presents the effect of rotational speed ω on the turbine overall size $d\_\max$ and net electric power output W_{net} As shown in Fig. 7, the effect of ω is considerably high on d_{max}. Increasing RPM from 30000 to 70000 reduces the turbine size by a maximum value of 46% for n-Pentane and isobutane. According to Eq. 1 and with constant ω, the rotor inlet radius r_4 is inversely proportional to ω and increasing RPM reduces r_4 and consequently d_{max}. On the contrary, W_{net} is not significantly affected by the variation of ω for all working fluids.

The effect of working fluid mass flow rate $\dot{m}$ on d_{max} and $\dot{W}_{net}$ is substantial as depicted in Fig. 8. With the rise of $\dot{m}$, the turbine efficiency and the actual enthalpy drop increase leading to larger r_4 based on Eq. 1. Conservation of mass at the rotor inlet achieves larger rotor inlet width b_4 and larger nozzle exit radius r_3 based on Eq. 31. Consequently larger d_{max} is achieved as shown in Fig. 8. The variation of $\dot{W}_{net}$ can be immediately related to Eq. 9 and Eq. 10. It is found from Fig. 8 that, lighter fluids can produce significantly larger power outputs (more than 54%) compared to the heavier (higher density) fluids while latter have smaller sizes due to their lower specific volumes.

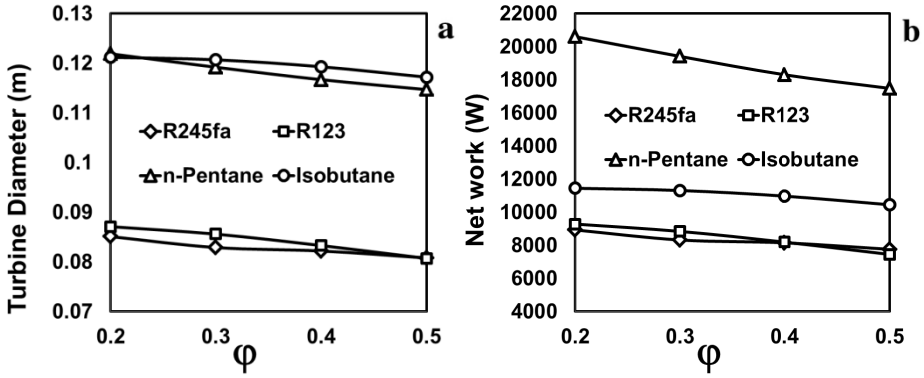

Figure 6 - Variation of coefficient ϕ.

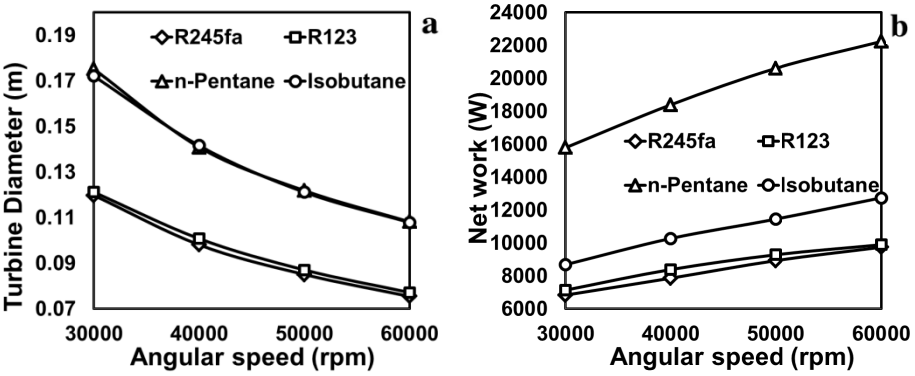

Figure 7. Variation of turbine speed ω.

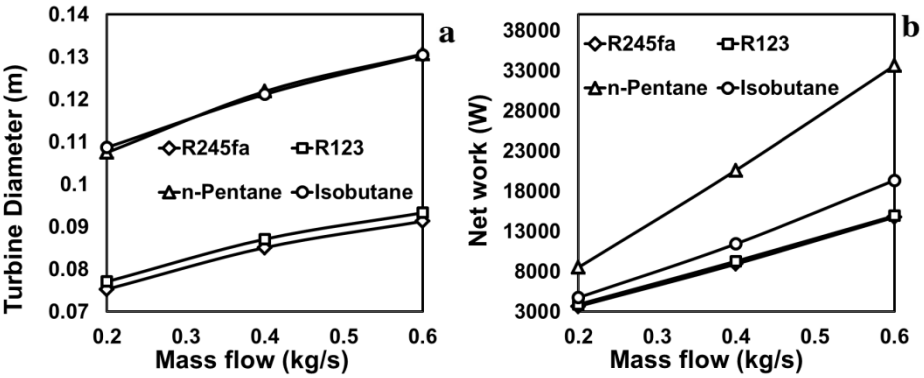

Figure 8. Variation of mass flow $\dot{m}$.

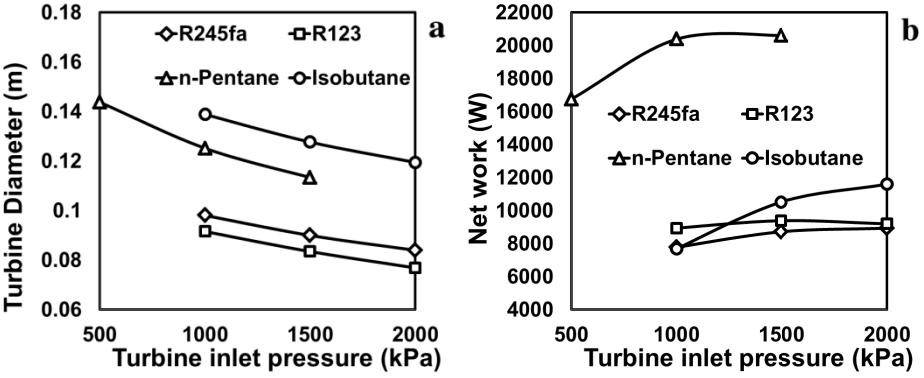

Figure 9. Variation of inlet pressure $P_{t,1}$.

Figure 9 shows that the effect of the turbine inlet total pressure $P_{t,1}$ on d_{max} and $\dot{W}_{net}$ is considerable. The upper boundary of pressure was chosen to be close to the fluid's critical pressure. As $P_{t,1}$ increases, the rotor inlet density q_4 increases leading to smaller rotor inlet width b_4 and consequently smaller r_3 is achieved (Eq. 31). With constant mass

flow rate, larger $P_{t,1}$ increases the turbine inlet density ρ_1 leading to smaller A_1 and r_1 according to Eq. 35 and Eq. 36 and consequently reduces d_{max} as shown in Fig. 3.4 a). On the contrary, increasing $P_{t,1}$ has negative effect on $\dot{W}_{net}$ of all working fluids with the maximum reduction of 45% for R245fa shown in Fig. 3.4 b). As $P_{t,1}$ increases the pump outlet pressure $P_{t,1} = P_7$ is also increased. At the same time the pump inlet density ρ_6 is reduced because of the higher condenser saturation temperature T_6. The accumulative effect of P_7 and ρ_6 increases $\dot{W}_{pump}$. On the other hand, increasing $P_{t,1}$ reduces Δh_{actual} which leads to smaller $\dot{W}_{turbine}$ and consequently reduces $\dot{W}_{net}$.

4. DISCUSSIONS AND CONCLUSIONS

The presented model allowed simulating important parameters for determining turbine characteristics. It also showed that some parameters have significant influence, such as angular velocity ω and mass flow ṁ. It was found also that the selected fluid have an important impact on performance of cycle. The model can be used to simulate the basic characteristics of radial inflow turbines. It is a good suggestion to adapt the model to use the optimal parameters obtained from a turbine to simulate off design operations. Other literature authors' models can be implemented for comparison and enhancement of the results.

5. ACKNOWLEDGEMENTS

Thanks to CAPES for the financial support to this research.

6. REFERENCES

Aungier RH. Turbine aerodynamics, axial-flow and radial-inflow turbine design and analysis. 1st ed. New York: ASME Press; 2006.

Bao, J., Zhao, L., A review of working fluids and expander selections for organic Rankine cycles. Renewable and Sustainable Energy Reviews, v. 24, p. 325-342, 2013.

BP. Statistical Review of World Energy. UK: Pureprint Group Limited;2018

Churchill SW. Friction-factor equation spans all fluid-flow regimes. Chem Eng 1977;84:91–2.

Chen, H., Goswami, D. Y., Stefanakos, E. K., A review of thermodynamic cycles and working fluids for the conversion low-grade heat. Renewable and Sustainable Energy Reviews, v. 14, p. 3059-3067, 2010.

Churchill SW. Friction-factor equation spans all fluid-flow regimes. Chem Eng 1977;84:91–2.

Clemente S, Micheli D, Reini M, Taccani R. Bottoming organic rankine cycle for a small scale gas turbine: a comparison of different solutions. Applyed Energy 2013;106:355–64

Fiaschi D, Manfrida G, Maraschiello F. Thermo-fluid dynamics preliminary design of turbo-expanders for ORC cycles. Appl Energy 2012;97:601–8.

Glassman AJ. Computer program for design and analysis of radial inflow turbines. NASA TN 8164; 1976.

Hettiarachchi HDM, Golubovic M, Worek WM, Ikegami Y. Optimum design criteria for an organic rankine cycle using low-temperature geothermal heat sources. Energy 2007;32:1698–706.

Moustapha H, Zelesky MF, Baines NC, Japikse D. Axial and radial turbines. 1st ed. White River Junction: Concepts NREC; 2003.

Rahbar, K., Mahmoud, S., Al-Dadah, R. K., Moazami, N. modelling and optimization of Rankine Cycle based on a small-scale radial inflow turbine. Energy conversion and management, v. 91, p. 186-198, 2014.

Rein, P., Engenharia do açúcar de cana. Editora Bartens, versão traduzida para o português, 2013.

Sauret E, Rowlands SA. Candidate radial-inflow turbines and high-density working fluids for geothermal power systems. Energy 2011;36:4460–7

Whitfield A, Baines NC. Design of radial turbomachines. 1st ed. New York: Longman; 1990.

7. RESPONSIBILITY NOTICE

The authors are the only responsible for the printed material included in this paper.